

# Mechanism of the double heterostructure $\text{TiO}_2/\text{ZnO}/\text{TiO}_2$ for photocatalytic and photovoltaic applications: A theoretical study

Slimane Haffad\*

*Département de Technologie, Faculté de Technologie,*

*Université A. Mira de Bejaia, Route Targa-Ouzemour, 06000 Bejaia, Algeria*

## Abstract

Understanding the mechanism of the heterojunction is an important step towards controllable and tunable interfaces for photocatalytic and photovoltaic based devices. To this aim, we propose a thorough study of a double heterostructure system consisting of two semiconductors with large band gap, namely, wurtzite ZnO and anatase  $\text{TiO}_2$ . We demonstrate via first-principle calculations two stable configurations of ZnO/ $\text{TiO}_2$  interfaces. Our structural study provides a key information on the nature of the complex interface and lattice distortions occurring when combining these materials. The study of the electronic properties of the sandwich nanostructure  $\text{TiO}_2/\text{ZnO}/\text{TiO}_2$  reveals that conduction band arises mainly from  $3d$  orbitals of  $\text{TiO}_2$ , while valence band is maintained by  $\text{O}_{2p}$  of ZnO, and that the trapped states within the gap region frequent in single heterostructure are substantially reduced in the double interface system. Unexpectedly, as a consequence of different bond distortions, the results on the band alignments show electron accumulation in the left shell of  $\text{TiO}_2$  rather than the right one. Such behavior provides more choice for the sensitization and functionalization of  $\text{TiO}_2$  surfaces.

PACS numbers:

Keywords: Density functional theory, ZnO/ $\text{TiO}_2$  interface, Photovoltaic, DSSC, Photocatalysis

## I. INTRODUCTION

Solar energy conversion consists on the production of electrical energy in the form of current and voltage from electromagnetic energy: i.e., incident light including infrared, visible, and ultraviolet (UV)<sup>1-6</sup>. The first generation solar cells were made of semi-conducting  $p-n$  junctions (based on Si wafers) and the second generation is based on the improvement of the first generation by employing thin film technologies<sup>1-3</sup>. In the last years, a third generation has emerged, which includes non-semiconductor technologies (polymer cells and biomimetics)<sup>2</sup>, nanowires (NWs) and quantum dots (QDs)<sup>3</sup>.

Within the third generation, dye sensitized solar cells (DSSCs) as low-cost solar cell, clean, and renewable energy sources became a practical root for photovoltaic cells when Regan and Graetzel<sup>4</sup>, in the late 1980s, have fabricated DSSCs composed of a porous layer of titanium dioxide ( $\text{TiO}_2$ ) nanoparticles immersed under an electrolyte solution and, covered with a dye molecule that absorbs sunlight. Such a technique expanded the use of semiconductors with wide band gap such as GaN,  $\text{SnO}_2$ , SiC, and ZnO which makes possible the conversion of higher energy photons. Ten years before this invention, A. Fujishima and K. Honda<sup>5</sup> discovered the effect of photosensitization of the  $\text{TiO}_2$  electrode under UV irradiation for the photocatalytic water splitting.

It is well known that interfacial charge recombination is a serious problem for photocatalytic and photovoltaic based devices<sup>1-3,6</sup>. Such a phenomena causes a loss of photo-generated electrons. It affects the open circuit voltage by decreasing the concentration of electrons in the conduction band of the semiconductor and, also the photo-current by decreasing the forward injection current. From this point of view, nanostructures, in regard of their large surface to volume ratio, present an inconvenience, i.e., by increasing the probability of charge recombination. An attempt to reduce the recombination rate consists of using a bilayer of a metal-oxide semiconductors electrode for high-performance nanomaterial-based DSSCs. One of the proposed systems are core-shell structures, which are derived from the nanoparticles and can reduce the charge recombination by forming a coating layer. An established electric field that may assist the separation of the electrons in the solid-solid interface can form energy barriers at the electrode-electrolyte interface. For this reason, several materials have been tested such as  $\text{SnO}_2/\text{TiO}_2$ <sup>7,8</sup>,  $\text{SnO}_2/\text{ZnO}$ <sup>9</sup>,  $\text{TiO}_2/\text{Nb}_2\text{O}_5$ <sup>10</sup>,  $\text{ZnO}/\text{Al}_2\text{O}_3$ <sup>11</sup>, and  $\text{ZnO}/\text{TiO}_2$ <sup>11,12</sup>. In the case of ZnO and  $\text{TiO}_2$ , their similar photovoltaic performances

did not come from similarity in properties but from compensating ones<sup>13</sup>. Matt Law *et al.*<sup>11</sup> demonstrated the superior performance of the ZnO/TiO<sub>2</sub> core-shell nanowire (CS-NWs) cells if compared to ZnO/Al<sub>2</sub>O<sub>3</sub> CS-NWs cells. Core-shell nanorod arrays based ZnO/TiO<sub>2</sub> encased in the hole-conducting polymer P3HT were performed and, a significant increases in the voltage and fill factor relative to devices without shells was observed<sup>14</sup>. In particular, Greene *et al.*<sup>14</sup> found that the shell-thickness affects the cell performance and, they showed that, adding a  $\sim 5$  nm polycrystalline TiO<sub>2</sub> shell improved the efficiency of the devices, while, Cr-doped TiO<sub>2</sub> nanoshell coating single-crystalline ZnO nanowires allows formation of *p-n* junctions via an efficient charge separation<sup>15</sup>. Park *et al.*<sup>16</sup> have realized photoelectrodes made of submicrometer-sized aggregates of ZnO nanocrystallites coated with TiO<sub>2</sub> layer by atomic layer deposition. They demonstrated that surface diffusion of the ZnO atoms at elevated annealing temperature can be suppressed and, the efficiency of DSSCs was enhanced with more than 30%. The effect of the interface ZnO/TiO<sub>2</sub> was also tested on the performance of polymer solar cells. It has been found that ZnO nanorod coated with TiO<sub>2</sub> layer demonstrates a significant reduction of the recombination rate and that the TiO<sub>2</sub> interface layer functions as an efficient photo-generated exciton quencher and assisted charge collection<sup>17</sup>. ZnO/TiO<sub>2</sub> hybrid nanostructures demonstrate also a higher catalytic activity<sup>18</sup>, where an enhanced charge transfer/separation process with fine interfaces was observed.

Understanding the mechanism of ZnO/TiO<sub>2</sub> heterojunction and how the physical characteristics are affected by the solid-solid reaction are crucial for a better use in photovoltaic or photocatalysis systems. Unfortunately, considering the lack of experimental data on the mechanism of the interface between ZnO and TiO<sub>2</sub>, we have based upon our own theoretical approach. However, some experimental studies were critical for the validation of our method. For example, Panigrahi and Basak<sup>19</sup> have found, using high resolution TEM (HRTEM) image, that the lattice fringes of ZnO/TiO<sub>2</sub> interface correspond to the (0002) plane of the wurtzite ZnO and to (112) plane of anatase (101) surfaces. One can draw similar observations from the works done by Wang *et al.*<sup>20</sup> and Greene *et al.*<sup>14</sup>. On the simulation level, to the best of our knowledge no work has been done in this perspective, except that in Ref.<sup>21</sup> in which the misfit between the different interfaces does not seem to reproduce the experimental situation mentioned above.

In this paper, we present electronic structure calculations of pseudo-realistic ZnO/TiO<sub>2</sub>

interfaces. Using density functional theory (DFT)<sup>22,23</sup> and, after a systematic study on the stability of the heterostructure, we analyze and discuss the effect of the distortions induced at the interfaces (interface hybridizations) owing to the misfit dislocations, in term of atomic bonding and relaxation. Next, we calculate the electronic properties of the sandwich system  $\text{TiO}_2/\text{ZnO}/\text{TiO}_2$ , in which the results are argued and compared to other available works. Afterward, we examine the alignment of the energy levels around valence and conduction bands by mean of an accurate method based on the average of the electrostatic potential<sup>24</sup>. At the end, a summary of the main results is presented. Our study provides a key information on the nature of the interfaces when matching together wurtzite ZnO with anatase  $\text{TiO}_2$  and their impacts on the band offsets.

## II. MODEL AND METHOD

The appropriate approach used to determine the stable interfaces is based on *ab initio* calculations where different orientations of  $\text{ZnO}/\text{TiO}_2$  heterostructure are combined. Previous theoretical and experimental studies evidence  $(10\bar{1}0)$  and  $(101)$  facets like the most stable surfaces for  $\text{ZnO}$ <sup>25</sup> and  $\text{TiO}_2$ <sup>26,27</sup>, respectively. Consequently, when bringing these two surfaces together, the interface will be:  $\text{ZnO } (10\bar{1}0) \parallel \text{TiO}_2 (101)$  or  $\text{TiO}_2 (10\bar{1})$ , that is, the mostly observed in experiment<sup>11,14,19,20</sup>. However, in literature published so far, few informations on the nature of the bonding and the presence or not of core dislocations were found. Nevertheless, It has been often noticed that ZnO core consists of a crystalline arrangement of atoms (hexagonal wurtzite structure), while  $\text{TiO}_2$  layers seem to be formed by polycrystalline and porous regions with anatase phase.

The  $\text{ZnO } (10\bar{1}0)$  non-polar surface is defined by the following lattice parameters:  $a_{\text{ZnO}} (//Y) \simeq 3.23 \text{ \AA}$ , and  $c_{\text{ZnO}} (//Z) \simeq 5.27 \text{ \AA}$  [see Fig. 1(a)], whereas the  $\text{TiO}_2 (10\bar{1})$  surface, also non-polar, is built by  $a_{\text{TiO}_2} (//Y) \simeq 3.78 \text{ \AA}$ , and  $c_{\text{TiO}_2-[101]} (//Z) \simeq 10.32 \text{ \AA}$ <sup>56</sup>. Based on the experimental observations<sup>14,19</sup> and structural information, we built our interface model by considering six (five) and two (one) unit cells in  $Y$  and  $Z$  directions, respectively, for  $\text{ZnO } (\text{TiO}_2)$  slabs. These parameters will be referred to as:  $A_{\text{ZnO}} = 6a_{\text{ZnO}} \parallel A_{\text{TiO}_2} = 5a_{\text{TiO}_2}$ ,  $C_{\text{ZnO}} = 2c_{\text{ZnO}} \parallel C_{\text{TiO}_2} = c_{\text{TiO}_2-[101]}$ . A combination of these two surfaces gives a reasonable lattice misfit less than 3%, with  $\frac{\Delta C}{C_{\text{TiO}_2}} \simeq \frac{\Delta C}{C_{\text{ZnO}}} \sim \pm 2.0 - 2.2\%$ , and  $\frac{\Delta A}{A_{\text{TiO}_2}} \simeq \frac{\Delta A}{A_{\text{ZnO}}} \sim \pm 2.7 - 2.8\%$ . To reproduce the experimental situation, we considered a periodically

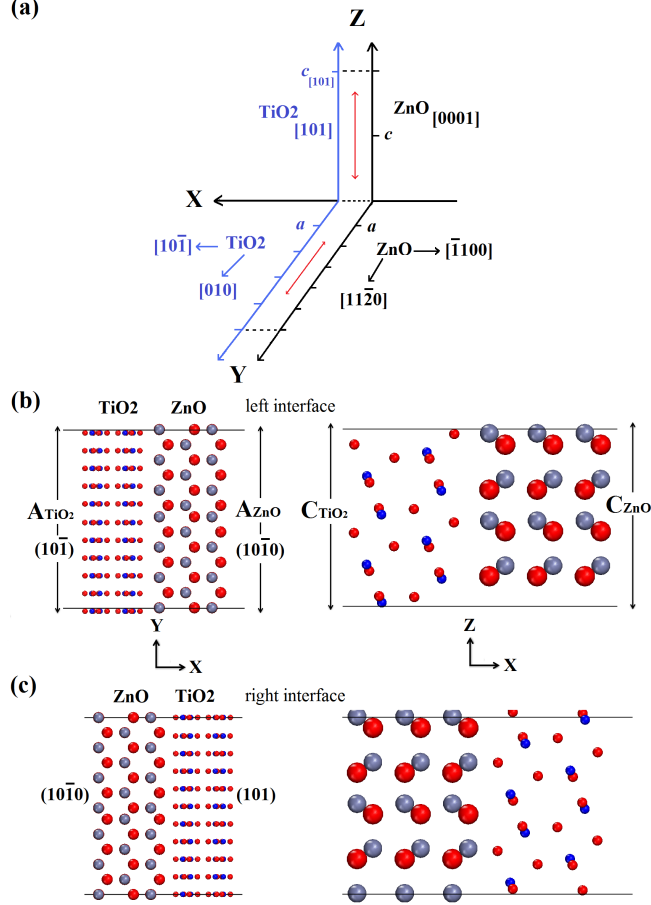


FIG. 1: Schematic representation in 3-D system of ZnO/TiO<sub>2</sub> interface (a), unrelaxed heterostructure of the left interface TiO<sub>2</sub>/ZnO (b), unrelaxed heterostructure of the right interface ZnO/TiO<sub>2</sub> (c). Oxygen, zinc, and titanium are represented by red, gray, and blue balls, respectively.

repeated multilayer: the interface was built by matching  $(6 \times 2)$  layers of ZnO  $(10\bar{1}0)$  with  $(5 \times 1)$  layers of TiO<sub>2</sub>  $(101)$ .

On the  $\text{TiO}_2\text{--}[101] \parallel \text{ZnO}_{[0001]}$  interface direction (in  $Z$  direction as labeled in Fig. 1), the TiO<sub>2</sub> super cell consists on eight parallel atomic layers of O and Ti<sup>57</sup> that matches with ZnO<sub>[0001]</sub> of eight parallel atomic layers (four of both O and Zn). Such a combination leads to an accordance with experimental observations deduced from the HRTEM image of Wang *et al.*<sup>20</sup> in which no core dislocation has been counted in this interface direction.

On the  $\text{TiO}_2\text{--}[010] \parallel \text{ZnO}_{[11\bar{2}0]}$  interface direction, the combination results in 10 and 12 slabs represented by the lattice parameters  $A_{\text{TiO}_2}$  and  $A_{\text{ZnO}}$ , respectively<sup>58</sup> (in  $Y$  direction as labeled in Fig. 1). This give rise to an edge dislocation in the supercell [two equivalent

TABLE I: The relative energies,  $E - E_{\min}$ , of the different configurations computed for various displacements,  $d$ , with respect to  $Z$  axis. Interface  $\text{TiO}_2/\text{ZnO}$ ;  $\text{TiO}_2$  slabs lie at the left side of  $\text{ZnO}$ , and interface  $\text{ZnO}/\text{TiO}_2$ ;  $\text{TiO}_2$  slabs lie at the right side of  $\text{ZnO}$ . The star indicates the most stable configurations

$\text{TiO}_2/\text{ZnO}$		$\text{ZnO}/\text{TiO}_2$	
$d$ ( $\uparrow z$ )	$E - E_{\min}$	$d$ ( $\uparrow z$ )	$E - E_{\min}$
( $\text{\AA}$ )	(eV)	( $\text{\AA}$ )	(eV)
-0.9	1.36	-0.9	2.42
-0.6	0.67	-0.6	0.09
-0.3	0.02	-0.3 ( $\star$ )	0.00
0.0 ( $\star$ )	0.00	0.0	1.95
0.3	0.37	0.3	6.20
0.6	1.02	0.6	10.37
0.9	1.18	0.9	13.63

dislocations lie at two different plans due to the very corrugated and sawtooth profile of the (101) surface of anatase  $\text{TiO}_2$ , see Ref.<sup>26</sup>].

Several tests were carried out in order to find and locate the stable configurations. Calculation tests were made by fixing the positions of  $\text{ZnO}$  ( $\text{TiO}_2$ ) atoms and displacing the coordinates of  $\text{TiO}_2$  ( $\text{ZnO}$ ) atoms in both  $Z$  and  $Y$  directions with  $0.3 \text{ \AA}$  until they coincide with the equivalent positions. We first moved the  $\text{TiO}_2$  ( $\text{ZnO}$ ) atoms in  $Y$  direction until the positions for which the minimum energy is reached, and then, by fixing the coordinates along  $Y$  at the minimal energy positions, the same procedure is followed for the  $Z$  direction.

The results on the interface orientations moved in  $Z$  directions are reported in Table I. From values of the energies, we identified two most stable orientations for which the minimum energy is obtained. To get the unrelaxed double interface system  $\text{TiO}_2/\text{ZnO}/\text{TiO}_2$ , we combined these two stables configurations in some sort of sandwich system in such a way that  $\text{ZnO}$  coated uniformly by  $\text{TiO}_2$  slabs: the two outer  $\text{ZnO}$  sides enclosed by (101) or (10 $\bar{1}$ ) surfaces of  $\text{TiO}_2$  (see Figs. 1 and 2). Our double heterostructure has a slab thickness of  $\sim 28 \text{ \AA}$  ( $\sim 15.7 \text{ \AA}$  of  $\text{ZnO}$  thickness and  $\sim 2 \times 6 \text{ \AA}$  for  $\text{TiO}_2$ ). By keeping the stoichiometry, the basic unit cell contains 528 atoms,  $\{(\text{ZnO})_{144} \text{ and } (\text{TiO}_2)_{80}\}$ , periodically repeated in

space within cubic boundary conditions separated by a vacuum region  $> 15 \text{ \AA}$  wide in  $X$  direction.

We employed the density functional theory (DFT)<sup>22,23</sup> method to investigate the properties of the sandwich system  $\text{TiO}_2/\text{ZnO}/\text{TiO}_2$ . Geometry relaxations are calculated within the generalized gradient approximation (GGA) as parameterized by Perdew, Burke, and Ernzerhof (PBE)<sup>28</sup>. The Kohn-Sham orbitals were expanded in numerical pseudo atomic localized basis sets (SIESTA package<sup>29</sup>) with double zeta polarization (DZP) and electron-ion interaction was included by employing norm-conserving pseudopotentials<sup>30</sup>. We used the zinc and oxygen pseudopotentials described elsewhere<sup>31</sup>, whereas a relativistic pseudopotential for the ionic titanium including non-linear core corrections was generated using the code ATOM<sup>32</sup> in the following reference configuration:  $3s^2 3p^6 3d^2 4f^0$ , with a cutoff radii of 1.5 a.u for  $3s$  and  $3d$ , 1.4 a.u for  $3p$ , and 2.0 a.u for  $4f$ . The states  $3s$  and  $3p$  of titanium were treated as semicore levels, whereas  $4s$  with  $3d$  were taken as higher valence states (12 valence electrons including the ionic charge). The Brillouin zone (BZ) sampling was performed using  $(16 \times 16 \times 16)$  and  $(1 \times 2 \times 4)$  Monkhorst-Pack grid<sup>33</sup> for bulk and slab models respectively, and a mesh cutoff of 500 Ry is considered in a real space grid. Structural optimizations were performed using the conjugate gradient method and convergence was assumed when the atomic forces were less than 0.03 eV.

### III. RESULTS AND DISCUSSIONS

Before presenting the results on the sandwich nanostructure, and for the sake of validation of our computational approach, we calculated the properties of ZnO and  $\text{TiO}_2$  in bulk systems. Within the above presented computational scheme, the lattice parameters computed for anatase  $\text{TiO}_2$  in bulk structure are  $a = 3.78 \text{ \AA}$  and  $c = 9.61 \text{ \AA}$  in very well agreement with experiment ( $a = 3.78 \text{ \AA}$ ,  $c = 9.50 \text{ \AA}$ )<sup>34</sup> and other theoretical calculations<sup>35</sup>. To address the accuracy of our method, we calculated structural parameters for  $\text{TiO}_2$  in rutile phase (with the same calculation parameters described above). The results are reported in Table II and in accordance with the previously published ones<sup>26,35,36</sup>. We found bulk anatase gives lower binding energy than that of rutile phase: our calculations give a notable similitude as compared to the experimental results. In fact, we found bulk rutile more stable than anatase phase of about 24 meV (0.55 Kcal/mol), which agrees with the experimental value

TABLE II: Calculated parameters for ZnO, anatase TiO<sub>2</sub>, and rutile TiO<sub>2</sub> in bulk structures at GGA (GGA+U) level:  $a$  and  $c$  are relaxed lattice parameters,  $E_g$  is the energy band gap.

	ZnO	anatase TiO <sub>2</sub>	rutile TiO <sub>2</sub>
$a$ (Å)	3.23 <sup>31</sup> (3.22)	3.78 (3.74)	4.59 (4.52)
$c$ (Å)	5.27 <sup>31</sup> (5.17)	9.61 (9.63)	2.97 (2.98)
$E_g$ (eV)	0.71 <sup>43</sup> (3.42)	2.03 (3.16)	1.82 (2.94)

of  $\sim 1.2$  Kcal/mol<sup>37</sup>.

It is well known that DFT-GGA describes the structural relaxation quite accurately, but fails to reproduce the correct alignment in the gap region, which leads to an underestimation of the band gap in the case of strongly correlated systems. To deal with a such inconvenience in the interface study, we performed GGA+U<sup>38</sup> calculations for ZnO wurtzite and TiO<sub>2</sub> in both anatase and rutile phases. After several trials, we identified the values of the effective potential,  $U$ , for which the experimental band gap and lattice parameters were successfully reproduced<sup>59</sup>. We found a suitable  $U_{O2p} = 2.4$  eV for the oxygen  $2p$  orbitals, and  $U_{Zn3d} = 8.0$  eV for  $3d$  orbitals of zinc, whereas for the  $3d$  orbitals of titanium, the effective potential shift  $U_{Ti3d} = 1.4$  eV. These parameters reduce the interaction between the valence band (VB) and conduction band (CB), and are used for the interface band structure calculations. The optimized lattice parameters for ZnO and TiO<sub>2</sub> in bulk systems at GGA+U level are reported in Table II (the values between brackets). The direct gap found in rutile is about 2.94 eV, while for the indirect gap in anatase phase is of 3.16 eV, in accordance with experiment<sup>39</sup>. The corresponding band dispersions along the high symmetry points, if compared to the ones obtained with GGA, are almost identical. The valence band width is slightly increased of 0.12 (0.05) eV for rutile (anatase). The O<sub>2s</sub> states are shifted up (around 1.5 – 1.8 eV) in both anatase and rutile structure, while in the case of ZnO, the  $3d$  electrons recover the correct alignments and found at  $\sim 7$  eV below the valence band maximum (VBM), approaching the experimental<sup>25</sup> and theoretical values obtained by employing hybrid functionals<sup>42</sup>. Furthermore, GGA+U calculations give also more accurate value of the relative energy  $\sim 55$  meV ( $\sim 1.27$  Kcal/mol), and very close to the experimental value<sup>37</sup> in which rutile phase is the most-*likely* stable under thermodynamic equilibrium conditions.



### A. Interface hybridization

Our final relaxed double heterostructure is depicted in Fig. 2. Both types of configurations (left and right interfaces) are characterized by two kinds of relaxation that have different interface hybridization. For example, at the left interface, the oxygen atom which lies at the core dislocation [labeled O1 in Figs. 2(b) and 3] relax inwards in both equivalent sites [surrounded by a circle in Fig. 2(b)], influencing thereby the connected atoms (Zn4 and Zn5 are pushed back, see Fig. 3). In contrast, at the right interface, the Ti atom located in front of Zn11 [labeled Ti11 in Figs. 2(b) and 3] relax outward with respect to titane planes causing bond distortions throughout the lattice (the dimer Zn11–O11 pushed inwards, see Fig. 3). Atoms of  $\text{TiO}_2$  in both sides of the surface undergo collective relaxation, whereas the ones at the interfaces form with those of ZnO a rhombohedron-*like* lattices (at the left heterojunction) and non-regular hexagonal-*like* lattices (at the right heterojunction) [see Figs. 2(b) and 3]. Surface relaxations of the outer layers are similar in both sides, identical to those characterizing the relaxation of (101) anatase  $\text{TiO}_2$ <sup>26,27</sup>, and the atoms therein (bulklike) are not affected by distortions that occur at interfaces.

If comparing atomic bond lengths in the relaxed system to those in the respective ideal-bulk structure of  $\text{TiO}_2$  and ZnO, one may note that these lengths are less distorted in the right interface than those of the left one (see Table III). Hence, the resulting total energy with GGA (GGA+U) of the right interface lower than that of the left one with about 2.6 (1.6) eV<sup>60</sup>. Some interface bond lengths and interatomic distances as labeled in Fig. 3 are summarized in Table III. The lengths of the dimers  $\text{O}_1\text{--Zn}_{1,4,5}$  at the left interface are contracted with respect to ZnO bulk value ( $\sim 1.98 \text{ \AA}$ <sup>43</sup>), whereas,  $\text{O}_2\text{--Zn}_{1,2}$  and  $\text{O}_3\text{--Zn}_{1,3}$  are larger. In contrast, at the right one, small bond distortions have been noticed (compare  $\text{O}_{11}\text{--Zn}_{11,12,13}$  &  $\text{Zn}_{11}\text{--O}_{12,13}$  lengths with  $1.98 \text{ \AA}$ ). It is worth noting that the left heterojunction presents two dangling bonds (O1 and its equivalent site), whereas in the right interface no dangling bonds were observed (see Fig. 3). Such structural changes induced by misfit dislocations entail the difference in total energy between the two interfaces, giving rise to an offset in the alignment of the energy levels between the two junctions as will presently appear below.

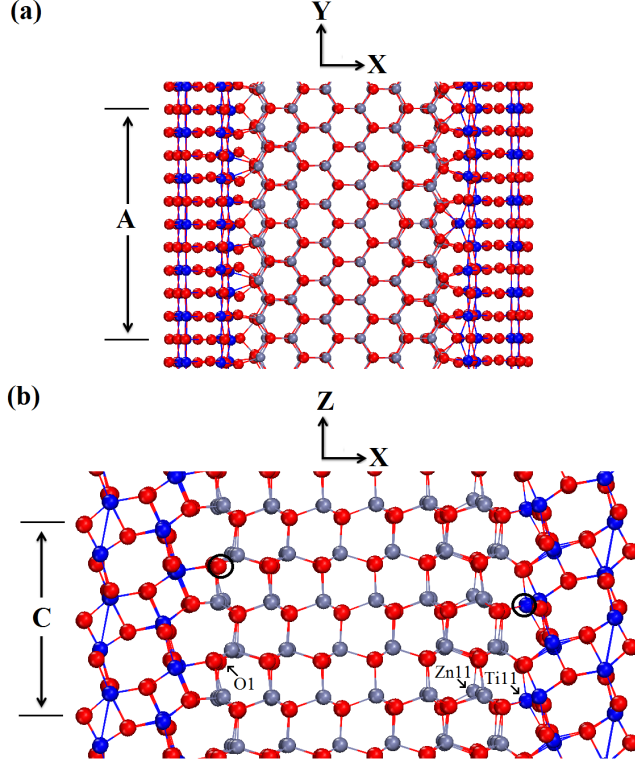


FIG. 2: Relaxed structure of the sandwich system  $\text{TiO}_2/\text{ZnO}/\text{TiO}_2$ : projection in  $(XY)$  plan (a), projection in  $(XZ)$  plan (b). Oxygen, zinc, and titanium are represented by red, gray, and blue balls, respectively.

TABLE III: Interatomic distances at the interfaces of the relaxed  $\text{TiO}_2/\text{ZnO}/\text{TiO}_2$  system. Atom labels refer to Fig. 3.

atomic label	length ( $\text{\AA}$ )	atomic label	length ( $\text{\AA}$ )
O1–Zn1	1.93	O11–Zn11	1.94
O1–Zn4	1.90	O11–Zn12	2.04
O1–Zn5	1.91	O11–Zn13	2.04
Zn1–O2	2.33	Zn11–O12	1.98
Zn1–O3	2.11	Zn11–O13	1.98
Zn2–O2	2.00	Ti11–O12	2.08
Zn3–O3	2.08	Ti11–O13	2.08
Ti1–O1	2.77	O12–O13	2.54

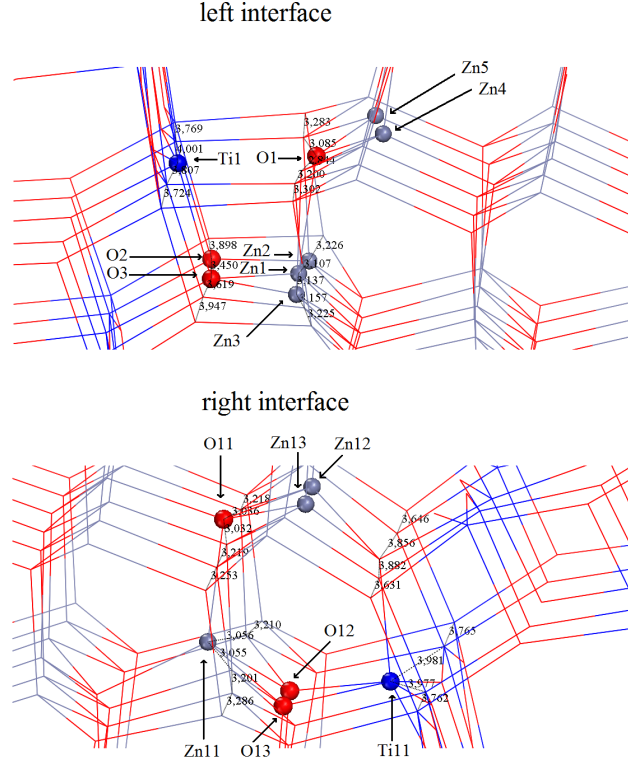


FIG. 3: Interface hybridizations and atomic bonding at the two interfaces of the relaxed  $\text{TiO}_2/\text{ZnO}/\text{TiO}_2$  system.

## B. Electronic properties

One of the queries, not yet properly explored from a simulation point of view, that we need to clarify is to overcome the band gap error in the interface band structure calculations. For this reason, we performed GGA+U simulations using the potential shift parameters carefully checked and described above. The band structure with the corresponding density of states (DOS) are reported in Fig. 4. The improvements made with respect to GGA results include: i) the direct energy gap is found more than twice larger [around 1.03 (2.53) eV with GGA (GGA+U)], ii) the electronic wave functions at the VB edges are localized, iii) the conduction band is mainly maintained by  $\text{Ti}_{3d}$  orbitals in which the 4s orbitals of zinc are pushed up [see Fig. 4(b)].

One of the palpable results of the sandwich system, if compared to a single heterostructure, can be observed from the DOS reported in Fig. 4(a). The trapped or interface states at the vicinity of VB are virtually eliminated, which states whose effects are detrimental

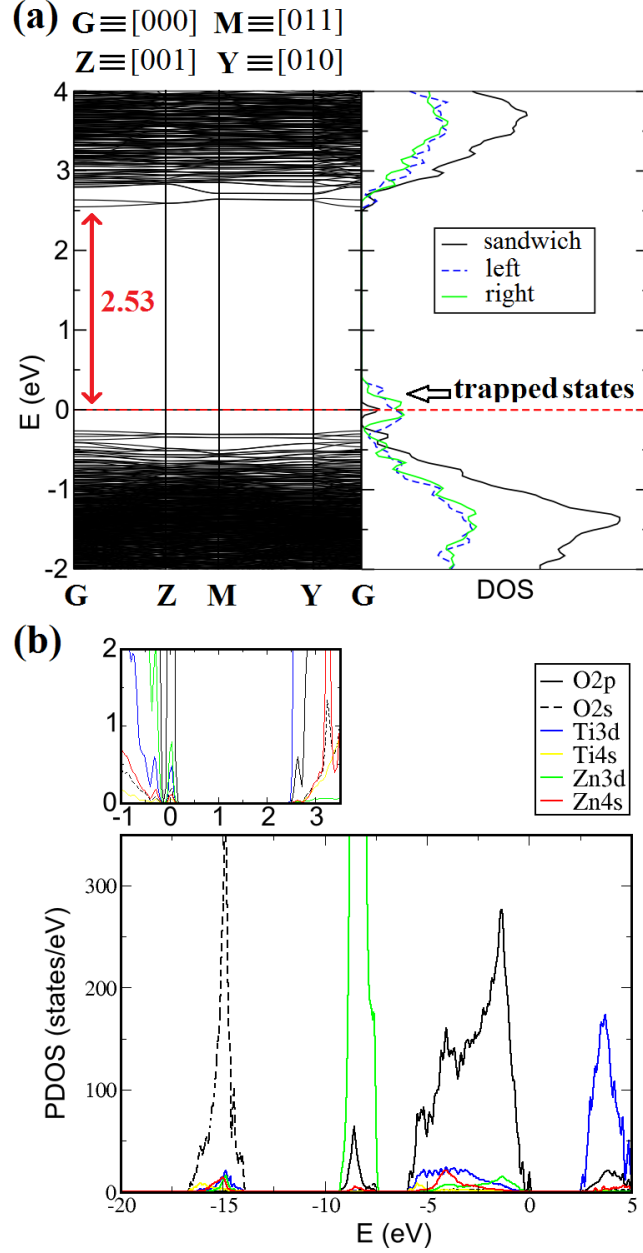


FIG. 4: Band structure plot along high symmetry points together with the total density of states, DOS, at GGA+U level, (the comparison between different densities is made by aligning their  $s$  and  $d$  states) (a), the projected density of states, PDOS, (b). The zero of energy is set to the VBM of the sandwich structure.

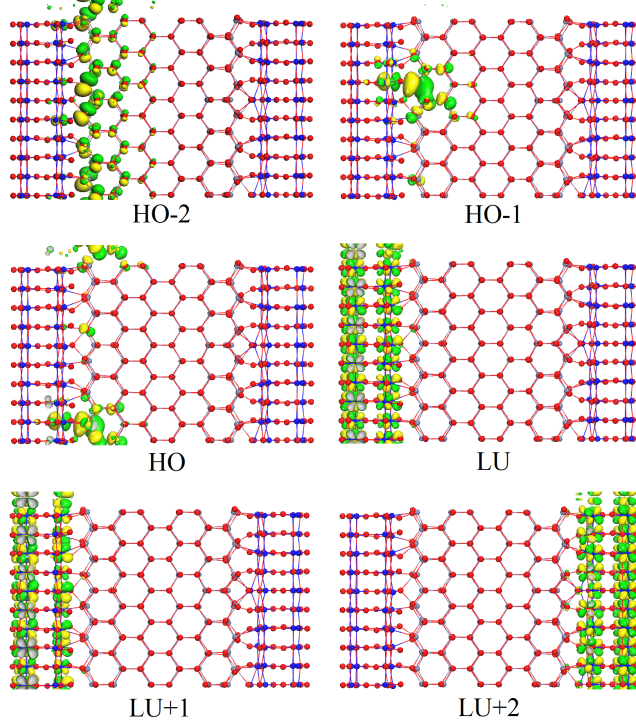


FIG. 5: Isosurface plots of the spatial distribution of the wave functions around VB and CB at Gamma-point as obtained for  $\text{TiO}_2/\text{ZnO}/\text{TiO}_2$  double heterostructure at GGA+U level. Isovalue of  $0.05 \text{ e}/\text{\AA}^3$ .

for the efficiency of the DSSC. Such behavior has been experimentally verified by many authors<sup>11,14,16–20,44–47</sup> but with inhomogeneous efficiencies. We have to underline that for an inverted sandwich structure, i.e.,  $\text{ZnO}/\text{TiO}_2/\text{ZnO}$ , the electronic and optical properties may behave differently due to the lower density of states in CB of  $\text{TiO}_2$  where the thickness of the two different materials affects significantly the band alignments as it was reported in Refs.<sup>46,47</sup>. Furthermore, it can be explained by the different electrostatic interaction at the semiconductor surface<sup>48</sup> and, unlike  $\text{ZnO}$ , in  $\text{TiO}_2$  the charge recombination is very slow. Němec et al.<sup>48</sup> attribute the different charge transport and recombination in the two semiconductors to the screening of the electrostatic interaction in  $\text{TiO}_2$  due to its high dielectric permittivity. In our case, one can also notice that the  $\text{ZnO}$  CB density shifted to higher energies by the larger density of 3d orbitals of titanium [see Fig. 4(b)], resulting in an increase of the excited electron lifetime.

Understanding the effect of atomic bonding and strains on the electronic states at the

edge of the VB and CB, the spatial distribution (wave functions) of some occupied and unoccupied states as obtained within GGA+U functional are plotted at Gamma-point [ $\Gamma$  as labeled in Fig. 4(a)] and illustrated in Fig. 5. One can see in clear the role of bonding and local atomic distortions on the overlap of the quantum states. In particular, the highest occupied state (HO) and (HO-1) are defect states that arise mainly from  $O1_{2p_{z,x}}$  and its likely-equivalent atom, respectively (localized on the core dislocations at the edge of the left interface). Whereas the lowest unoccupied state (LU) and (LU+1) derived mainly from  $Ti_{3d}$  orbitals of titane atoms of the left heterojunction: this finding evidences that the conduction band potential of the left interface is more negative than that of the right one. The conduction band of  $TiO_2$  in both sides of the double interface is more negative than that of  $ZnO$  at variance to what have been suggested in Refs.<sup>21,44</sup>. Yet, other experimental results reported in Refs.<sup>18,49,50</sup> in which  $TiO_2$  CB is found more negative than  $ZnO$  CB are consistent with our GGA+U predictions.

### C. Interface band offsets

To dispel doubts over the above issue and, for a better and clear description of the relative positions of energy levels at the interfaces<sup>61</sup>, a lineup of the average of the electrostatic potential between the two materials is required. To define band offsets: valence band offset (VBO) and conduction band offset (CBO), we employ the method described in Refs.<sup>51–53</sup>. These are calculated according to the following relation:  $VBO (CBO) = \Delta E_v (\Delta E_c) + \Delta V$ , where  $\Delta E_v$  ( $\Delta E_c$ ) is the so-called *band-structure* term, which refers to the difference between the top (bottom) of the valence (conduction) bands as obtained from two independent bulk band structure calculations.  $\Delta V$  is the lineup of the average of the electrostatic potential through heterojunctions. The quantity  $\Delta V$  contains all interface effects that result from electronic charge transfer after interfacial hybridization (induced by the electric dipole).

The plot of the average of the electrostatic potential is illustrated in Fig. 6(a). In this case, only the VBO is calculated from the double-macroscopic average technique, and by using the above formula, we deduce CBO by adding the experimental gap of the materials constituting our sandwich structure.

The computed values are depicted schematically in Fig. 6(b). They evidence an heterojunction type II, in agreement with experimental observations<sup>18,49,50,54,55</sup>. The larger energy

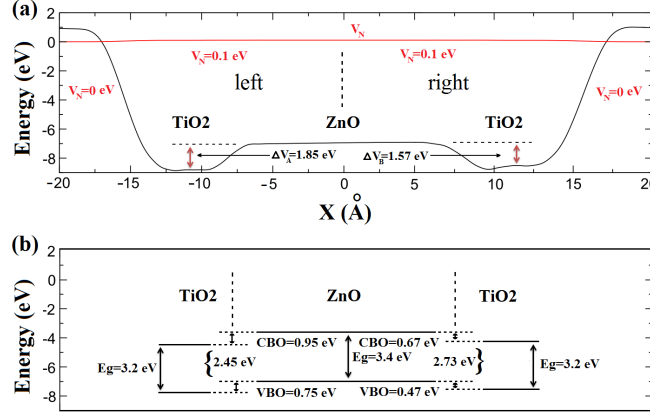


FIG. 6: Diagram of the average of the Hartree potential and the neutral potential  $V_N$  as obtained using the double-macroscopic average technique (a). Schematic representation of the valence band offsets (VBO) and conduction band offsets (CBO) for TiO<sub>2</sub>/ZnO/TiO<sub>2</sub> interfaces (b). The energy gap,  $E_g$ , refers to the experimental gap of bulk systems.

gradient between CB (VB) of ZnO and CB (VB) of TiO<sub>2</sub> favors the transfer of the excited electrons (active holes) from ZnO (TiO<sub>2</sub>) to TiO<sub>2</sub> (ZnO). The striking feature regards the difference in band offsets between the left and right interfaces, in which the conduction band potential of the left side is more negative with about  $\sim 0.23 - 0.28$  eV, and thereby leading to an electron accumulation in the CB of the left shell of TiO<sub>2</sub> rather than the right one. The VBO (CBO) is found to be 0.75 (0.95) eV and 0.47 (0.67) eV for the left and the right interface, respectively (see Fig. 6), predicting a more enhanced charge transfer/separation for the case of the left interface structure. The above result points to challenges in fabricating a double heterojunction with desirable interfacial structures, since inappropriate structures of the interface can lower the desired properties of the hybrid materials<sup>18</sup>. This result also reveals to what extent the potential of valence and conduction bands can be modified by interfacial effects, and may explain why there have been controversial published results<sup>18,21,44,47,49,50</sup> as well as on the energy band alignments and on the effect of ZnO coating layer on the device performance of a DSSC.

It is worthwhile to note that the minimal gap calculated from the double-macroscopic average technique [ $\sim 2.45$  eV from Fig. 6(b)] close to the gap value given by GGA+U calculations [ $\sim 2.53$  eV, see Fig. 4(a)]. Moreover, the LU+2 state maintained by Ti<sub>3d</sub> of the right side of TiO<sub>2</sub>/ZnO/TiO<sub>2</sub> system (see Fig. 5) is found at 2.71 eV above VBM,

[HO→(LU+2)], nearly to what we estimated from the gap region of the right interface  $\sim 2.73$  eV [see Fig. 6(b)]. The above remarks demonstrate the accuracy of our GGA+U results and validate the double-macroscopic average technique for the determination of the band offsets in semiconductor/semiconductor interfaces.

In the experimental results published so far, several works pointed out qualitatively<sup>11,14,18,49,55</sup> the band alignments between the two materials but does not allow a direct comparison. To the best of our knowledge, some values on ZnO/anatase-type TiO<sub>2</sub> heterojunction band offsets have been obtained by Ran Zhao *et al.*<sup>50</sup>, that are of 0.2 (0.6) eV for CBO (VBO), quantitatively closer to what we found for the right interface. Similar results were found in Ref.<sup>54</sup> in which the CBO estimated to be 0.44 eV for 0.7 nm thick ZnO that decreases upon thickness expansion of ZnO. While measurements on wurtzite ZnO/rutile-type TiO<sub>2</sub> by x-ray photoelectron spectroscopy (XPS)<sup>49</sup> evaluate VBO (CBO) to be  $0.14 \pm 0.05$  ( $0.45 \pm 0.05$ ) eV.

#### IV. CONCLUSIONS

In summary, an extensive study on the nature of the interface between ZnO (wurtzite) and TiO<sub>2</sub> (anatase) has been presented by means of DFT(+U) simulations. Our structural analysis allowed us to obtain; an accordance between the atomic planes of the two materials in the TiO<sub>2</sub>-<sub>[101]</sub> || ZnO<sub>[0001]</sub> interface direction, and a misfit dislocation in the perpendicular direction TiO<sub>2</sub>-<sub>[010]</sub> || ZnO<sub>[11 $\bar{2}$ 0]</sub>, in agreement with experimental observations<sup>11,14,19,20</sup>. Using the ground state energy calculations, we found two most stable configurations that have different interface hybridization, from which our double heterostructure TiO<sub>2</sub>/ZnO/TiO<sub>2</sub> has been constructed. Besides, the non-equivalence of the atomic environment and the presence of more dangling bonds in the left interface makes it less stable than the right one. The study of the electronic properties at GGA+U level shows that valence band is maintained by O<sub>2p</sub> orbitals of ZnO, whereas conduction band arises mainly from 3d orbitals of titanium in which Zn<sub>4s</sub> were slightly pushed up. Furthermore, by using the double-macroscopic average technique, we evidence an heterojunction type II but we observed a worthy difference in energy levels between the two interfaces (left and right), resulting in an electron accumulation in the CB of the left shell of TiO<sub>2</sub> rather than the right one. Such a double interface system demonstrates an efficient charge separation and increasing of



excited electron lifetime, in particular, when  $\text{TiO}_2$  is used as a shell with a suitable thickness. In practical point of view, despite of the difficulty to experimentally realize such interface orientations, and for the multiple advantages mentioned above,  $\text{ZnO}/\text{TiO}_2$  heterostructures offer a better possibility of use in photocatalytic and photovoltaic based devices, especially the sandwich structure  $\text{TiO}_2/\text{ZnO}/\text{TiO}_2$ .

## Acknowledgments

I would like to thank Dr. G. Cicero from polytechnic of Turin for helpful discussions, remarks and advice. The author is grateful to the South African Center for High Performance Computing (CHPC) and CINECA Award N. HP10CLG9UX, 2011 for the availability of high performance computing resources and support.

---

\* Electronic address: slimanehaffad@gmail.com

- <sup>1</sup> Stephen J. Fonash, *Solar Cell Device Physics*, Elsevier, 30 Corporate Drive, Suite 400, Burlington, MA 01803, 2nd ed., USA, (2010).
- <sup>2</sup> Songjun Li, Jagdish Singh, He Li, and Ipsita A. Banerjee, *Biosensor Nanomaterials*, Wiley-VCH Verlag & Co. KGaA, Boschstr. 12, 69469 Weinheim, Germany, (2011).
- <sup>3</sup> Matt Law, Joshua Goldberger, and Peidong Yang, *Annu. Rev. Mater. Res.* 34, 83 (2004).
- <sup>4</sup> Brian O'Regan and Michael Grätzel, *Nature* 353 (6346), 737 (1991).
- <sup>5</sup> A. Fujishima and K. Honda, *Nature* 238, 37 (1972).
- <sup>6</sup> Y. Diamant, S. Chappel, S. G. Chen, O. Melamed, and A. Zaban, *Coord. Chem. Rev.* 248, 1271 (2004).
- <sup>7</sup> S. Chappel, S. G. Chen, and A. Zaban, *Langmuir* 18, 3336 (2002).
- <sup>8</sup> Chuanwei Cheng, Yee Yan Tay, Huey Hoon Hng, and Hong Jin Fan, *J. Mater. Res.* 26, 17 (2011).
- <sup>9</sup> N. G. Park, M. G. Kang, K.M. Kim, K. S. Ryu, S. H. Chang, D. K. Kim, J. van de Lagemaat, K. D. Benkstein, and A. J. Frank, *Langmuir* 20, 4246 (2004).
- <sup>10</sup> K. Sayama, H. Sugihara, and H. Arakawa, *Chem. Mater.* 10, 3825 (1998).
- <sup>11</sup> Matt Law, Lori E. Greene, Aleksandra Radenovic, Tevye Kuykendall, Jan Liphardt, and Pei-

- dong Yang, J. Phys. Chem. B 110, 22652 (2006).
- <sup>12</sup> Chun-Yu Lee, Jen-Yi Wang, Yi Chou, Meng-Yueh Liu, Wei-Fang Su, Yang-Fang Chen, and Ching-Fuh Lin, J. Appl. Phys. 107, 034310 (2010).
  - <sup>13</sup> Aravind Kumar Chandiran, Mojtaba Abdi-Jalebi, Mohammad K. Nazeeruddin, and Michael Grätzel, ACS Nano 8 (3), 2261 (2014).
  - <sup>14</sup> Lori E. Greene, Matt Law, Benjamin D. Yuhas, and Peidong Yang, J. Phys. Chem. C 111 (50), 18451 (2007).
  - <sup>15</sup> T. D. Dao, C. T. T. Dang, G. Han, C. V. Hoang, W. Yi, V. Narayanamurti, and T. Nagao, Appl. Phys. Lett. 103, 193119 (2013).
  - <sup>16</sup> Kwangsuk Park, Qifeng Zhang, Betzaida Batalla Garcia, and Guozhong Cao, J. Phys. Chem. C 115, 4927 (2011).
  - <sup>17</sup> Mi-Jin Jin, Junhyeon Jo, Ji-Hee Kim, Ki-Seok An, Mun Seok Jeong, Jeongyong Kim, and Jung-Woo Yoo, ACS Appl. Mater. Interfaces 6, 11649 (2014).
  - <sup>18</sup> Chun Cheng, Abbas Amini, Chao Zhu, Zuli Xu, Haisheng Song, and Ning Wang, Scientific Reports 4, 4181 (2014).
  - <sup>19</sup> Shrabani Panigrahi and Durga Basak, Nanoscale 5, 1925 (2011).
  - <sup>20</sup> Meili Wang, Changgang Huang, Yongge Cao, Qingjiang Yu, Zhonghua Deng, Yuan Liu, Zhi Huang, Jiquan Huang, Qiufeng Huang, and Wang Guo, J. Phys. D: Appl. Phys. 42, 155104 (2009).
  - <sup>21</sup> José C. Conesa, J. Phys. Chem. C 116 (35), 18884 (2012).
  - <sup>22</sup> P. Hohenberg and W. Kohn, Phys. Rev. B 136, 864 (1964).
  - <sup>23</sup> W. Kohn and L. J. Sham, Phys. Rev. 140, 1133 (1965).
  - <sup>24</sup> A. Baldereschi, S. Baroni, and R. Resta, Phys. Rev. Lett. 61, 734 (1988).
  - <sup>25</sup> Ü. Özgür, Ya. I. Alivov, C. Liu, A. Teke, M. A. Reshchikov, S. Doğan, V. Avrutin, S.-J. Cho, and H. Morkoç, J. Appl. Phys. 98, 041301 (2005).
  - <sup>26</sup> Michele Lazzeri, Andrea Vittadini, and Annabella Selloni, Phys. Rev. B 63, 155409 (2001).
  - <sup>27</sup> Xue-Qing Gong, Annabella Selloni, Matthias Batzill, and Ulrike Diebold, Nature Materials 5, 665 (2006).
  - <sup>28</sup> J. P. Perdew, K. Burke, and M. Ernzerhof, Phys. Rev. Lett. 77, 3865 (1996).
  - <sup>29</sup> José M Soler, Emilio Artacho, Julian D Gale, Alberto García, Javier Junquera, Pablo Ordejón, and Daniel Sánchez-Portal, J. Phys.: Condens. Mater 14, 2745 (2002).

- <sup>30</sup> N. Troullier and J. L. Martins, Phys. Rev. B 43, 1993 (1991).
- <sup>31</sup> S. Haffad, M. Samah, and G. Cicero, Phys. Rev. B 85, 165207 (2012).
- <sup>32</sup> A. Garcia, ATOM User's Manual. Version 3.2, July (2002).
- <sup>33</sup> H. J. Monkhorst and J. D. Pack, Phys. Rev. B 13, 5188 (1976).
- <sup>34</sup> J. K. Burdett, T. Hughbanks, G. J. Miller, J. W. Richardson, Jr., and J. V. Smith, J. Am. Chem. Soc. 109, 3639 (1987).
- <sup>35</sup> De Nyago Tafen and James P. Lewis, Phys. Rev. B 80, 014104 (2009).
- <sup>36</sup> Amilcare Iacomino, Giovanni Cantele, Fabio Trani, and Domenico Ninno, J. Phys. Chem. C 114, 12389 (2010).
- <sup>37</sup> David R. Lide, ed., *CRC Handbook of Chemistry and Physics*, 90th ed. (CRC Press/Taylor and Francis, Boca Raton, FL, 2010), CD-ROM version.
- <sup>38</sup> S. L. Dubarev, G. A. Botton, S. Y. Savrasov, C. J. Humphreys, and A. P. Sutton, Phys. Rev. B 57, 1505 (1998).
- <sup>39</sup> H. Tang, F. Lévy, H. Berger, and P. E. Schmid, Phys. Rev. B 52, 7771 (1995).
- <sup>40</sup> A. Beltran, J. R. Sambrano, M. Calatayud, F. R. Sensato, and J. Andrès, Surface Science 490, 116 (2001).
- <sup>41</sup> Juan C. Garcia, Micheal Nolan, and N. Aaron Deskins, J. Chem. Phys. 142, 024708 (2015).
- <sup>42</sup> S. J. Clark, J. Roberson, S. Lany, and A. Zunger, Phys. Rev. B 81, 115311 (2010).
- <sup>43</sup> S. Haffad, G. Cicero, and M. Samah, Energy Procedia 10, 128 (2011).
- <sup>44</sup> Simelys Hernández, Valentina Cauda, Angelica Chiodoni, Stefano Dallorto, Adriano Sacco, Diana Hidalgo, Edvige Celasco, and Candido Fabrizio Pirri, ACS Appl. Mater. Interfaces 6 (15), 12153 (2014).
- <sup>45</sup> Jinxia Duan, Jiamin Wu, Jun Zhang, Yang Xu, Hao Wang, Di. Gao, and Peter D. Lund, International Journal of Energy Research 40 (6), 806 (2016).
- <sup>46</sup> G. Torrisi, A. Di Mauro, M. Scuderi, G. Nicotra, and G. Impellizzeri, RSC Adv. 6, 88886 (2016).
- <sup>47</sup> Ghobadi A., Ulusoy T. G., Garifullin R., Guler M. O., and Okyay A. K., Scientific Reports 6, 30587 (2016).
- <sup>48</sup> H. Němec, J. Rochford, O. Taratula, E. Galoppini, P. Kužel, T. Polívka, A. Yartsev, and V. Sundström, Phys. Rev. Lett. 104, 197401 (2010).
- <sup>49</sup> Jun Wang, Xiang-Lin Liu, An-Li Yang, Gao-Lin Zheng, Shao-Yan Yang, Hong-Yuan Wei, Qin-Sheng Zhu, and Zhan-Guo Wang, Applied Physics A 103, 1099 (2011).

- <sup>50</sup> Ran Zhao, Liping Zhu, Fangping Cai, Zhiguo Yang, Xiuquan Gu, Jun Huang, and Ling Cao, Appl. Phys. A 113, 67 (2013).
- <sup>51</sup> Javier Junquera, Magali Zimmer, Pablo Ordejón, and Philippe Ghosez, Phys. Rev. B 67, 155327 (2003).
- <sup>52</sup> L. Colombo, R. Resta, and S. Baroni, Phys. Rev. B 44, 5572 (1991).
- <sup>53</sup> M. Peressi, N. Binggeli, and A. Baldereschi, J. Phys. D 31, 1273 (1998).
- <sup>54</sup> Kai Shen, Kunjie Wu, and Deliang Wang, Materials Research Bulletin 51, 141 (2014).
- <sup>55</sup> Hua Cai, Peipei Liang, Zhigao Hu, Liqun Shi, Xu Yang, Jian Sun, Ning Xu, and Jiada Wu, Nanoscale Research Letters 11, 104 (2016).
- <sup>56</sup> These are lattice parameters optimized for bulk calculations.
- <sup>57</sup> In fact, these atomic layers are spaced by the lattice fringes characterizing (112) planes of anatase (10 $\bar{1}$ ) or (101) surfaces of TiO<sub>2</sub>.
- <sup>58</sup> Our theoretical deductions are in agreement with the HRTEM image of the work done by Matt Law *et al.*<sup>11</sup>, from which we counted 33 atomic planes of ZnO corresponding to 27 atomic planes of TiO<sub>2</sub>. Our analysis of the crystallographic and image data attributes this interface direction to TiO<sub>2</sub>-<sub>[010]</sub>  $\parallel$  ZnO<sub>[11 $\bar{2}$ 0]</sub>.
- <sup>59</sup> It should be known that the appropriate choice of  $U$  depends on several parameters namely: the DFT code used, the choice of basis sets, pseudopotentials, and K-points mesh<sup>41</sup>.
- <sup>60</sup> It should be noted here that we also made relaxations for the two interfaces separately, i.e., for TiO<sub>2</sub>/ZnO (left) and ZnO/TiO<sub>2</sub> (right).
- <sup>61</sup> Even if we can have an idea about band alignments around valence and conduction bands from results obtained with GGA+U functional, it is necessary to confirm or refute it by using another method namely double-macroscopic average technique<sup>24,52,53</sup>.